Proceedings of ASME Turbo Expo 2011
GT2011
June 6-10, 2011, Vancouver, British Columbia, Canada

GT2011-45163

NUMERICAL SIMULATION OF SURGE IN TURBOCHARGER CENTRIFUGAL COMPRESSOR – INFLUENCES OF DOWNSTREAM PLENUM

Dr Strong Guo[1], Dr Hua Chen[2], Dr Xiaocheng Zhu[3], Professor Zhaohui Du[3]
1. Honeywell Technology Solutions (China), Shanghai 201203, China
2. Honeywell Turbo Technologies Ltd, UK; 3. Shanghai Jiaotong University, China
hua.chen@honeywell.com

ABSTRACT

Surge is an important instability seriously affecting compression systems. This paper presents a numerical simulation of surge flow phenomenon inside a turbocharger centrifugal compressor with a vaneless diffuser. The compressor was discharged into a plenum and the effect of the plenum on surge behavior of the compressor system was investigated. The entire geometry of the compressor, including the impeller, vaneless diffuser, volute housing and downstream plenum, were included in the simulation. Three-dimensional Reynolds averaged compressible Navier–Stokes equations were solved with the k–ε turbulence model using commercial software CFX and two different sizes of plenum were studied. A new plenum model is proposed which allows temporal variation of temperature inside the plenum. The numerical technique employed to set up CFD (computational fluid dynamics) with such an unstable flow system are described. The results show that when the plenum volume was nearly doubled, the dominating frequency of the system suddenly dropped from 72Hz to 23Hz. During the surge cycle, the compressor characteristic (pressure ratio v mass flow curve) showed distinct differences. With the smaller plenum, the characteristic showed random traces with little global backflow at the compressor inlet, while with the larger plenum, clear surge cycles are displayed with strong global backflow at the inlet. The flow fields of the two systems are presented as functions of time and show distinct differences. In the case of the smaller plenum, the circumferential flow field inside the impeller is non uniform, showing influences of rotating stall, while in the case of the large plenum, the circumferential uniformity returns and the flow field behaves quasi-steadily during the surge cycle. With the larger plenum, the volute flow synchronises with the inlet mass flow oscillation in time and a completed vortex break down occurs at every volute cross section, but with the smaller plenum the synchronisation disappears and vortex break down only occurs partially at the centers of some volute cross sections.

NOMENCLATURE

Letters:

A	***Area, Volute throat section area***, m^2
B	***Axial dimension of flow passage***, m
C	***Plenum constant (Fig.1B)***, $(s \cdot K \cdot m)^{-1}$
D	***Diameter***, m
$\dot{m}$	***Mass flow rate***, kg/s
P	***pressure***, Pa
S	***Entropy***, J/K
t	***Time***, s
u	***Flow velocity in plenum***, m/s
V	***Volume in plenum***, m^3
R	***Centroid radius of volute throat***, m ***specific gas constant***, J/(kg*K)

Subscripts

1	***Compressor inlet***
2	***Impeller leading edge***
3	***Impeller trailing edge***
4	***Diffuser exit***
5	***Volute discharger***
h	***Hub***
t	***Tip, shroud***
6	***Plenum outlet***
p	***Plenum***

Greek letters

δ	***Small increment***
Δ	***Increment***
ρ	***Density***, kg/m^3
γ	***Specific heat capacity ratio***

1. INTRODUCTION

Surge is an unstable flow phenomenon that affects the entire centrifugal compression system (the centrifugal compressor, inlet and outlet piping, downstream plenum or storage tank and the control valves). It is characterized by a limited cyclic oscillation with large amplitude fluctuations of the mean flow through the system. Because of the large fluctuations of pressure and mass flow rate it creates, and its unstable flow nature, surge can result in total loss of performance of the compressor. Furthermore, the power level of the pressure oscillations can approach that of the compressor itself, inducing large mechanical loads on the system which can lead to mechanical failure. Moreover, during part of the surge cycle, the mean mass flow may reverse. This reversal and the fluctuations in pressure and flow rate can pose a threat to any processes or machines connected. In contrast to surge, stall is a local phenomenon of the compressor. When stall occurs, there are regions of relatively low flow that form at isolated locations inside the compressor. In other words, surge maybe regarded as a one-dimensional system instability while stall is a multi-dimensional compressor instability. Therefore the time scale of surge is significantly larger than that of stall.

There have been a large number of studies on surge and stall phenomena in both axial and centrifugal compressors in the open literature, a few of them are quoted here. Classic work by Moore and Greitzer[1, 2] established the Moore-Greitzer surge model in which the compressor rotor and stator are treated as an actuator disk that has the same effects on the flow as the compressor itself. The model employs three partial differential equations to describe the behavior of the system (the model can handle rotating stall as well). More recent works by Mezic[3] and by Birnir *et al*[4] further extended the model to include an eddy viscosity term. Others included Fink *et al*.[5], Gravdahl *et al*.[6], Kang *et al*.[7], Levy *et al*.[8], Longley[9], Paduano *et al*.[10], Senoo *et al*.[11] and Spakovszky[12]. In these studies, surge was defined as instability of the entire system resulting in an oscillation of pressure and mass flow in anti-phase. The occurrence of surge under any given operating condition was dependent on the B-parameter in the Moore-Greziter model (Greitzer[13]). Coupled modes of stall and surge were also found (Rose *et al*.[14]), although at high speeds the system behavior was usually dominated by surge and no coherent stall cells were detected (Schleer & Abhari[15]).

Due to the violent flow nature of surge, making detailed flow field measurements during surge is very difficult, particularly at high compressor speeds. Few studies have been published in open literature (NASA 2001[16]). Computational fluid dynamics (CFD) has been used in the design of centrifugal compressors and in the analysis of their flow field for several decades. It would seem therefore that the method might be a useful tool to simulate surge, and the behavior and detailed flow field of a compressor at surge. However, application of the CFD to centrifugal compressor surge is far from easy. Firstly the most commercial CFD codes were written mainly for steady flow calculations while surge is an unsteady flow phenomenon; even for those with some capacity for handling internal unsteady flow, simplifications are usually made in the treatment of boundary conditions at flow domain boundaries. As large areas of flow separation are also expected in surge, convergence of simulations is not guaranteed. Secondly, surge is a system wide phenomenon so the entire compression system, including impeller, diffuser, volute housing/collector, inlet and outlet piping systems, needs to be incorporated in the simulation. Note that all the rotor blade passages, diffuser passages and entire volute may need to taken into account. Thirdly, depending on system configuration, the time scale of a surge cycle is usually about 10~100 times longer than that of compressor stall. These make surge calculation very lengthy and difficult. Many researchers have opted for simpler 1-D and 2-D codes to simulate rotating stall and surge e.g. references[17~19]. Niazi *et al*[20] in 2000 developed a 3-D compressible unsteady flow solver to analyze surge of a centrifugal compressor and to study steady and pulsed air injection control of the compressor stability. The same method was also used[21] to simulate axial compressor surge and air injection control. M. Vahdati *et al*[22] in 2006 did an unsteady simulation of an Aero-engine core compressor during rotating stall and surge. The researchers acquired the surge frequency and observed not only flow reversal into the low pressure compression domain, but also that the surge loops in terms of its mass flow vs pressure characteristic.

In references[23, 24], the present authors solved the unsteady, 3-D Navier-Stokes flow within a turbocharger centrifugal compressor stage. A plenum model was added at the housing exit to simulate the components downstream of the compressor, and CFX commercial software was used. In the present study, we extended the method to study surge in the compressor and its compression system, with special focus on the influence of downstream plenum volume. The geometry of the compression system will be described, and then the methodology of the simulations detailed. The results of the simulations will then be presented and discussed.

2. GEOMETRY OF COMPRESSION SYSTEM

The compressor studied is a Honeywell turbocharger centrifugal compressor model GT70 with vaneless diffuser and volute housing. The main geometric parameters of the compressor and its operating condition are given in **Table 1**.

Table 1 Compressor studied	
Wheel type	Centrifugal
Blade number	6 full blades & 6 splitter blades
Wheel inducer tip diameter (D2t)	133.15mm
Wheel inducer hub diameter (D2h)	44.60mm
Wheel exducer tip diameter (D3t)	182.88mm
Wheel axial length (tip, L2t)	58mm
Wheel axial length (hub, L2h)	61.4mm
Diffuser exit diameter (D4)	304.8mm
Diffuser axial gap (B4)	12.13mm
Ratio of volute throat area to the centroid radius of the volute throat A/R	34.29mm
Volute discharge diameter (D5)	99mm
Wheel corrected rotational speed (n)	44198rpm (44.2krpm)
Corrected mass flow rate at plenum exit ($\dot{m}_6$)	1kg/s

For turbocharger compressors used in road vehicles, their inlet and outlet piping systems are much shorter than compressors used for processing industry, due to limited space within vehicles. The lengths of the pipes can sometime be of the same order as the compressor flow path. Focusing on the effect of downstream piping and to simplify the simulation task, the inlet pipe for the compressor is ignored in the present study, and a plenum is connected to the compressor volute housing directly. A throttle valve is placed at plenum outlet to control the mass flow rate of the compressor. **Fig. 1A** shows the compressor modeled with a computational grid, and **Fig. 1B** shows the plenum model. Two plenums with differing volumes of $0.0909m^3$ and $0.1591m^3$ were simulated. The larger volume is equal to the volume of compressor outlet pipe in the gas-stand test rig that produced the compressor performance map in **Fig. 2**, while the smaller volume is closer to that found in engine setup environment.

3. NUMERICAL TECHNIQUES

3.1 Governing equations and CFD code

Three-dimensional, Reynolds averaged compressible Navier–Stokes equations are solved using version 12 of commercial CFD software CFX[25] together with the k–ε turbulence model. One consideration in preferring the k–ε turbulence model to other two-equation turbulence models is its ability to include solid surface roughness in simulations. Surface roughness of 0.0032mm for the impeller and diffuser and 0.0063mm for the volute were included in the present simulation.

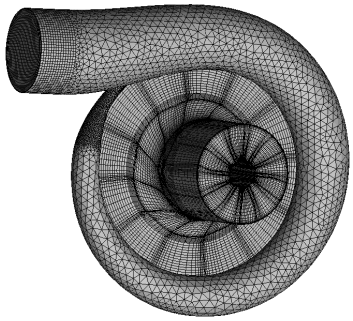

Fig. 1A Compressor & computational grid

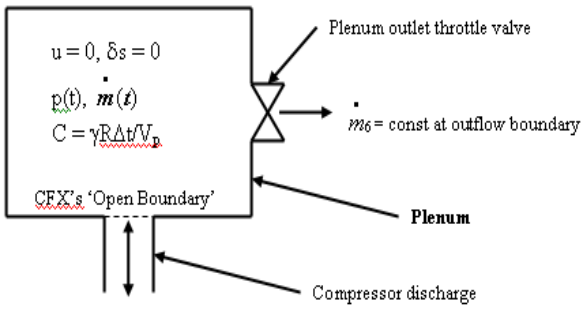

Fig. 1B Downstream plenum

3.2 Computational mesh and numerical setup

The computational mesh is shown in **Fig. 1A**. The entire compressor including all six impeller flow passages was modelled. This is necessary because the flow in the impeller is not necessarily circumferentially uniform, nor is the influence this exerts on the downstream components. For impeller and diffuser flow passages, a structured mesh was used. The O-type mesh was employed near the impeller blades, and mean y+ value was about 20. The H-type mesh was adopted in the other parts of the passages. An independent H-type mesh was used in the impeller blade tip clearance. The minimum mesh angle is 16deg. For the volute, an unstructured tetrahedral mesh was generated with refinement around the tongue region. A structured mesh was employed for the short inlet and outlet pipes. The total number of computational cells is just 0.753 millions. Computational time required for surge simulation is very lengthy, so it is important to balance the need for accuracy and need for computational efficiency. Since the frequency of surge is an order smaller than the impeller rotational frequency, and the purpose of the present work is to capture the main flow feature of the surge and not the

details of it, the use of such a coarse mesh is justified. A non-slip condition was imposed on all the solid walls. Near the solid walls, the scalable wall function[25] was used. In unsteady simulations, the transient rotor/stator interface[25] was adopted between wheel outlet and vaneless diffuser inlet.

The physical time step was set to 2.2625×10^{-5}s. This corresponds to a pitch angle of 6° at the given rotational speed. The impeller has six main blades and six splitter blades, so it takes ten time steps for inducer blades to rotate a blade pitch and five time steps for exducer blades to do the same. This time step was found to be sufficient to produce converged results that catch both stall and surge of the compressor. The number of iterations for internal loop, that is, the number of iterations spent at each physical time, was chosen to be 10. Note that this number and the physical time step both have significant influence on the required computational time and convergence of the calculations. Usually, the larger this number is, the better the convergence will be, but also the longer the time will be. The calculations were carried out in two stages: a steady flow simulation was first carried out and the results were used as initial conditions for subsequent unsteady simulations.

3.3 Inlet and outlet boundary treatments

Under surge conditions, large flow reversals at both inlet and outlet of the compressor are possible. Traditional boundary treatments for steady flow simulations cannot handle these reversals. Therefore, the "opening boundary" method in CFX[25] was selected. At the inlet, the "opening pressure for entrainment" scheme was selected. In this scheme when the flow direction is into the domain, the pressure value is taken to be the total pressure (that is, total pressure is imposed) based on the velocity component normal to the boundary. When it is leaving the domain, it is taken to be the static pressure (that is, static pressure is imposed). At the outlet of the compressor (not the plenum), the "static pressure for entrainment" scheme was selected. In this scheme the pressure value is taken to be the static pressure for both the inflow and outflow, and flow direction is obtained by enforcing the velocity gradient perpendicular to the boundary to be zero. "Opening temperature" and "opening static temperature" schemes were also used at the inlet and the outlet respectively.

The imposed inlet boundary conditions were steady and consisted of spatially uniform total pressure and total temperature. The flow to the inlet was assumed normal to the inlet cross-section. A mass flow rate was imposed at the outlet of the plenum.

3.4 Plenum model

A plenum, **Fig. 1B**, was commonly used to simulate the large gas receiver or storage tank often located at downstream of the compressor. An assumption was made that the volume of the plenum is constant (in reality when charging an internal combustion engine, cylinder volume of the engine changes with time). The flow inside the plenum was assumed to be isentropic, spatially uniform, and to have negligible velocity. It was also assumed that the fluid flowed out of the plenum through a throttle valve at various preset mass flow rates. This approach allowed temporal variation of static pressure at the compressor outlet boundary under surge condition. However, unlike the conventional plenum model in which the static temperature inside the plenum is assumed constant, the present plenum model allows the temperature to vary with time and this gives a more realistic description of what happens inside the plenum. With inflow to the plenum from the compressor, only static pressure of the plenum is imposed at the compressor outlet boundary, other flow variables including static temperature at the boundary are calculated using flow information inside compressor and are likely to vary with time. Assuming constant plenum temperature will cause contradictions. So the plenum constant C that describes the characteristic of the plenum is revised to be $\gamma R \Delta t / V_p$, where γ and R are the ratio of specific heats and specific gas constant of the fluid, Δt is the physical time step in CFD runs, and V_p is the volume of the plenum. In this study, air was the fluid, and values of 1.4 and 287J/(kg·K) were used for γ and R respectively, and the physical time step was set to 2.2625×10^{-5}s. Two C values, 0.1 /(s·K·m) and 0.05712/(s·K·m) which corresponds to two plenum volumes of 0.0909 m^3 and 0.1591m^3 respectively, were used to analyse the effect of the plenum.

4 RESULTS AND DISCUSSIONS

4.1 Compressor stage performance

Computed and experimental total pressure ratios are given in **Fig. 2**. Measured surge flow at 44.2krpm is 1.07kg/s and the CFD results are given at 1.0k/s for the two plenums. Unsteady flow calculations were used and the computed performances were time averaged results. When the C value is equal to 0.1 (the smaller plenum), calculated total pressure ratio agrees reasonably well with the experimental data. The CFD result has a slightly higher value and this is expected as certain physical features of the compressor such as the leakage flow between the compressor impeller back disc and compressor housing were not included in the simulation. In the larger plenum case (C = 0.05712), predicted the total pressure ratio is much lower than that of the smaller plenum. The monitored inlet and outlet mass-averaged total pressure histories of the CFD are given in **Fig. 3**. It shows why the same compressor with a larger plenum has inferior performance at surge. At the outlet, the total pressure fluctuation is larger and the mean value of the pressure is lower with the larger plenum. Also at the

inlet, the mean value of total pressure is higher with the larger plenum due to a stronger reverse flow.

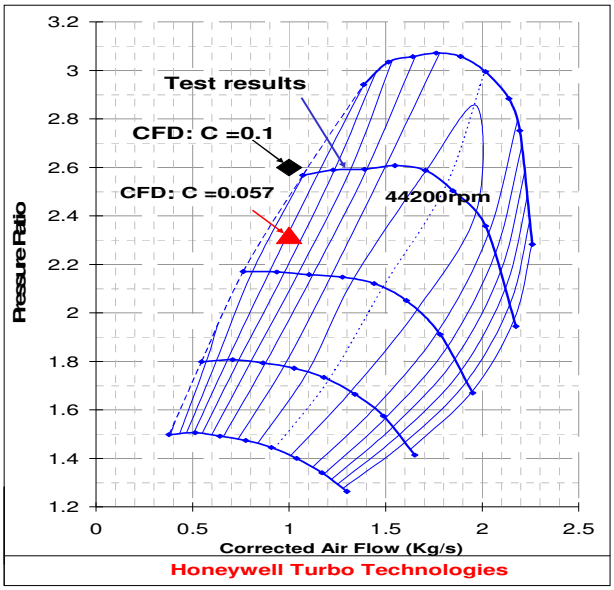

Fig. 2 Computed & measured compressor characteristic

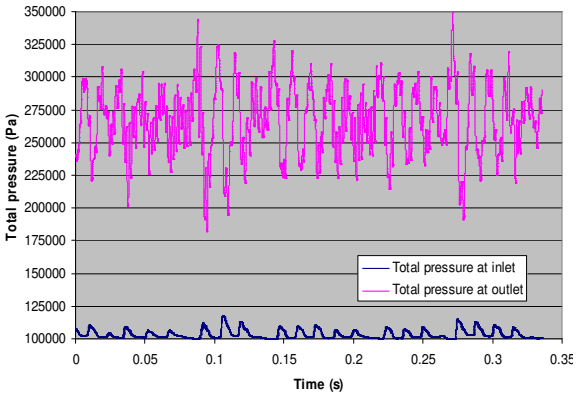

C =0.1, smaller plenum

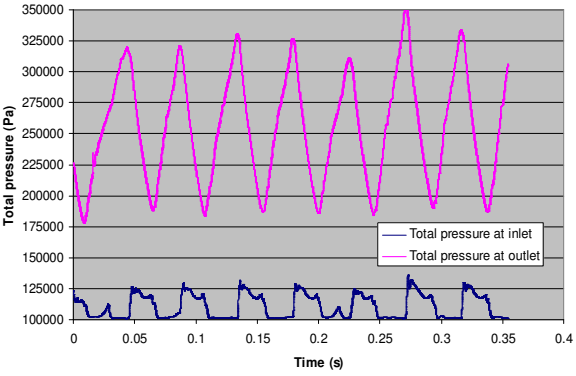

C =0.05712, larger plenum

Fig. 3 Total pressure histories at inlet and outlet, mass flow rate =1.0kg/s

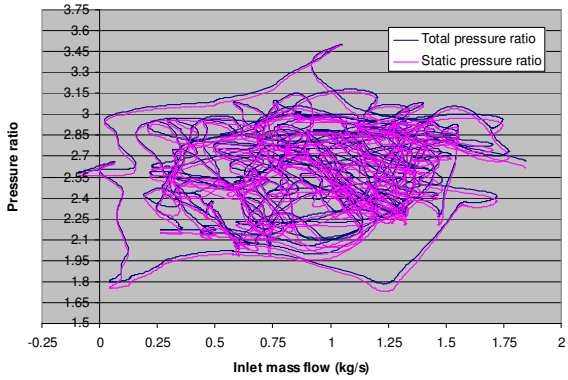

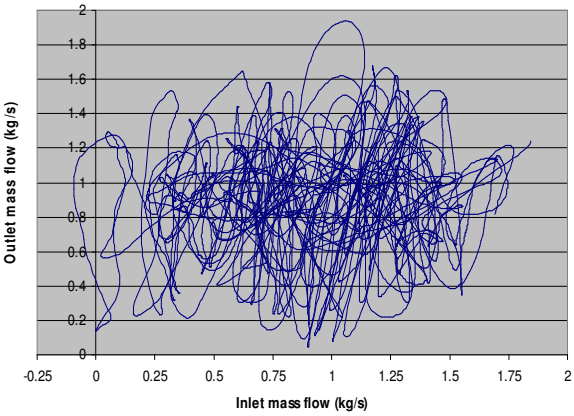

C =0.1

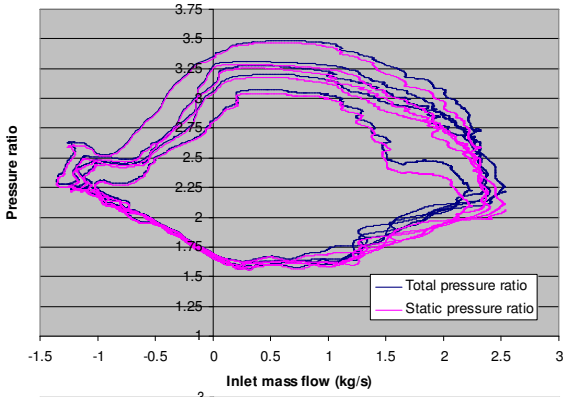

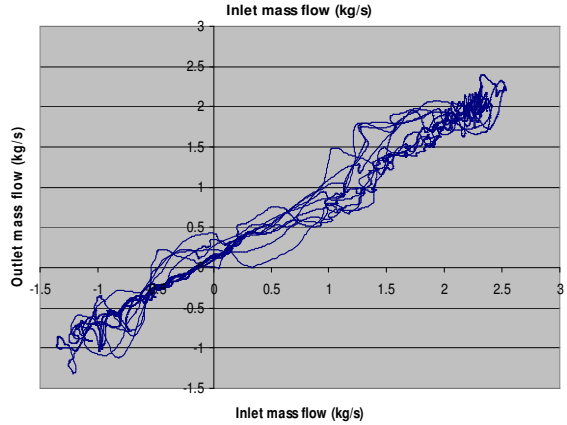

C=0.05712

Fig. 4 Surge cycles for different C values

4.2 Surge cycle of different plenums

During surge cycles, the compressor total pressure ratio and static pressure ratio vs. inlet mass flow and inlet mass flow vs. outlet mass flow are given in **Fig. 4**. 14 and 5 cycles are shown for the smaller and the larger plenums respectively. The characteristics of the smaller plenum do not show clear cyclic patterns, and while there are some global reverse flows at the compressor inlet, there is no back flow at the compressor outlet. Additionally, there is no obvious synchronization between the inlet and outlet mass flows. For the larger plenum, however, the pressure ratio-mass flow characteristics display a clear cyclic pattern, and there is significant back flow at the compressor outlet as well as at the inlet. A clear relationship between the inlet flow and outlet flow is also shown. The relationship is close to linear, indicating a single dominating flow phenomenon. The frequency of this phenomenon is lower (See **Fig. 3**) than those encountered with the smaller plenum.

4.3 Spectrum Analysis of pressure in vaneless diffuser

A monitoring point was set up half way inside the vaneless diffuser (**Fig. 5**) during the simulation in order to catch the changes in flow variables with time at the diffuser. The static pressure fluctuations at the point and their FFT (Fast Fourier Transfer) analysis results are given in **Fig. 6**. The periodical oscillations of the pressure are mainly established with frequencies of 71.6Hz and 22.6Hz. With the larger plenum, the 22.6Hz oscillation dominates over the other frequencies, and its amplitude is much larger than that of the largest oscillation with the smaller plenum. With the smaller plenum, there are many higher frequencies disturbances, such as at 319Hz, 531Hz etc. Note that the rotating frequency of the impeller is 736.6Hz, and the blade passing frequency of the impeller is 4419.8Hz and 8839.6Hz for the inducer blades and exducer blades respectively.

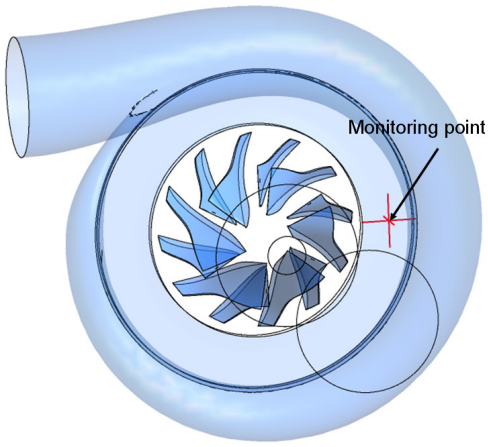

Fig. 5 Monitoring point inside diffuser

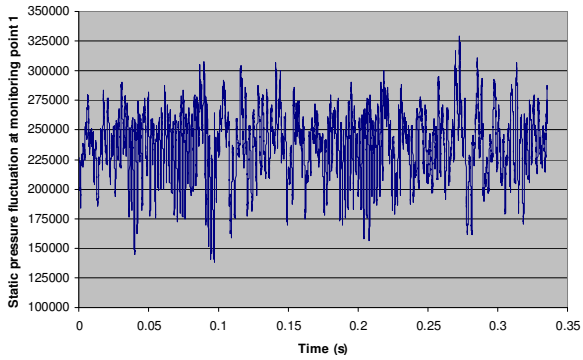

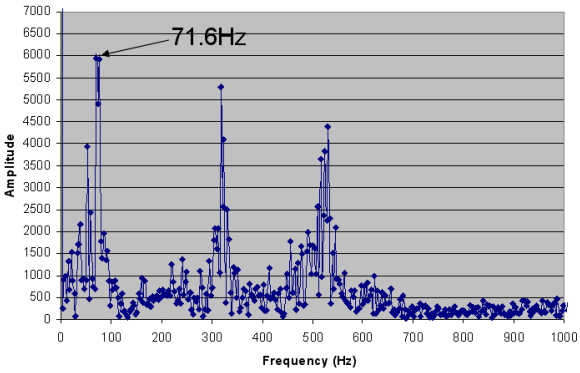

C=0.1

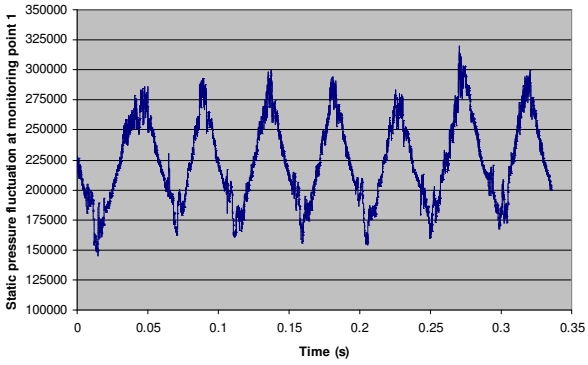

C=0.05712

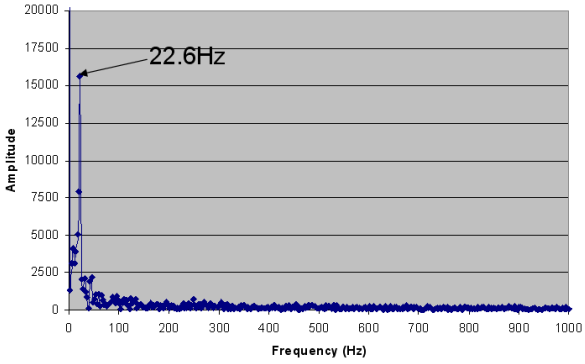

C=0.05712

Fig. 6 Static pressure fluctuation at monitoring point and FFT analysis results

Combined with the results presented in references[23, 24], the effect of plenum volume on the dominating frequency of the compression system is further shown in **Fig. 7**. Note that the frequency for the largest C value is acquired at a mass flow rate of 1.1kg/s and not 1.0kg/s. However since mass flow rate has little effect on the surge/stall frequency, this small inconsistency does not affect the validity of the results. As can be seen from **Fig. 7,** something dramatic happens when the C value is reduced from 0.1 to 0.057. It seems that when C = 0.1 (and larger) the system was in a rotating stall condition, but when C = 0.057, the system went into surge.

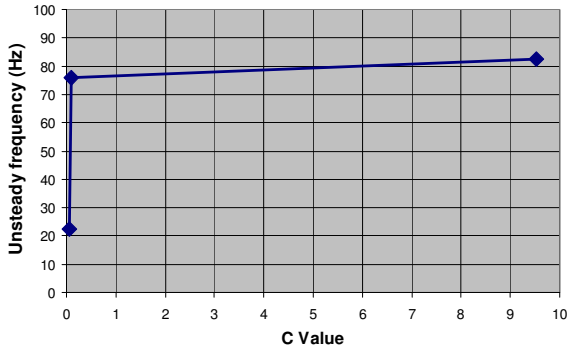

Fig. 7 Effect of plenum volume on system dominating frequency

4.4 Unsteady flow fields in the wheel

Five different time instants during the surge cycle are marked in **Fig. 8**. Relative velocity contours at 90% span of rotor passages projected to the blade-to-blade plane are given in **Fig. 9**. For both the C values, the variety of flow fields at different instants of surge cycles can be seen clearly and in general the flow behaves quasi-steadily. The quasi-steadiness is due to the wave length of the 71.6Hz and 22.6 Hz oscillations being far greater than that of the blade pitch. The flow fields in the diffuser and volute show that the oscillation involves the entire compressor stage. But the difference is also clear between the two plenums. When the C value is 0.1, circumferential variations in the flow field between different blade channels are distinct at every time instant (a feature of rotating stall), but it is accompanied by a longer wave disturbance. When the C value reduces to 0.05712, the flow field circumferential variations between different blade channels are very small at every instant, and flows in all the channels are more or less synchronous to the stronger, lower frequency disturbance that dominates the whole compressor stage.

4.5 Unsteady flow fields in the diffuser

Radial velocity contours in the diffuser at 50% span at the five different time instants are given in **Fig. 10**. The tongue of the housing is shown at the top left-hand corner in each graph and the compressor wheel rotates anticlockwise. In references[23, 24], the present authors found that when a compressor stage goes into stall, a standing wave may appear in the volute and at the diffuser exit, creating a circumferentially twin-peaked velocity distribution in the diffuser. This distribution remains during the stall cycle. Current results with a C value of 0.1 are similar to this finding. However, when the C value is reduced to 0.05712, this flow phenomenon disappears. It is also clear from **Fig. 10** that when the C value is 0.1, flow only partially reverses in the diffuser. But when the C value is reduced to 0.05712, the entire flow can reverse in the diffuser (time instant 3).

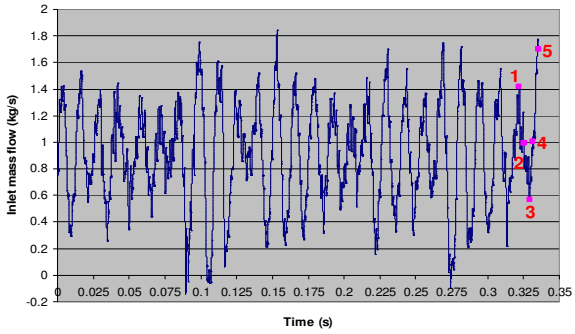

C=0.1

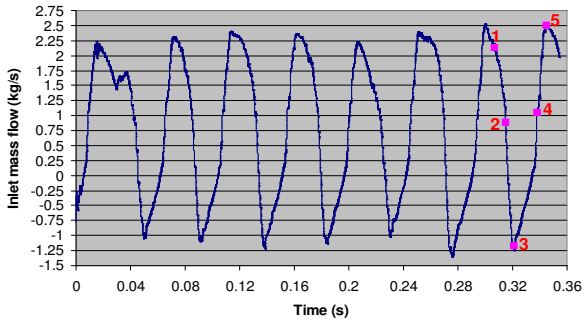

C=0.05712

Fig. 8 Computed compressor inlet mass flow oscillation

4.6 Unsteady flow fields in the volute

Tangential velocity contours at five circumferential locations in the volute (shown in **Fig. 11**) are given in **Fig. 12** for the five time instants. Cross sections 1 to 4 are each 90 deg apart and located inside the volute proper, and cross section 5 is located in the volute discharge section. The direction of the flow is out of the paper. Note that in these plots *positive values means reversed flows*. When the C value is 0.1, the flow partially reverses at cross section 5 at time instant 2 when the compressor inlet mass flow rate obtains its cyclic mean of 1kg/s (**Fig. 8**). Note that the inlet flow reaches its minimum at time instant 3 so there is a

time or phase difference between inlet mass and outlet mass flows. When the C value is reduced to 0.05712, the flow field becomes more regular, showing dominance of one long-wave disturbance. Note that the inlet and outlet flows both reverse at time instant 3 and the flow reversal is also stronger than that with the smaller plenum.

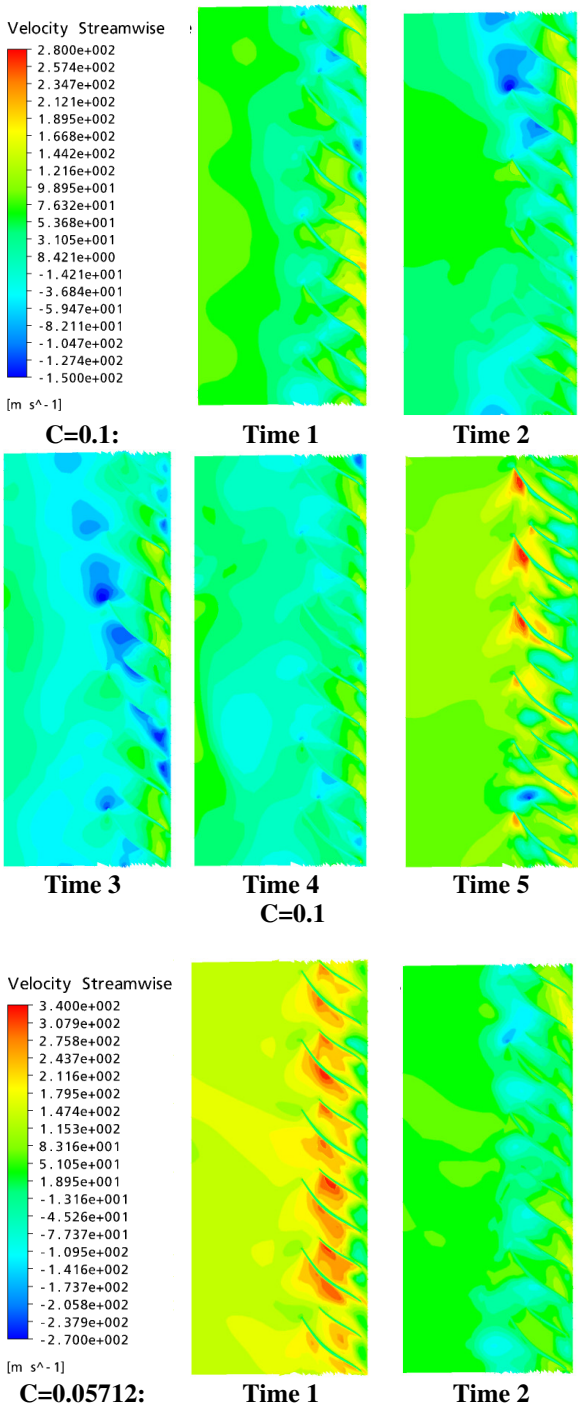

Fig. 9 Streamwise velocity contour in wheel, 90% blade span at five different time instants

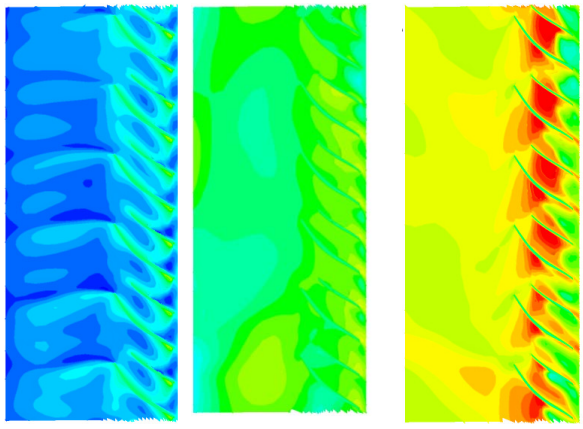

Fig. 9 Cont'd

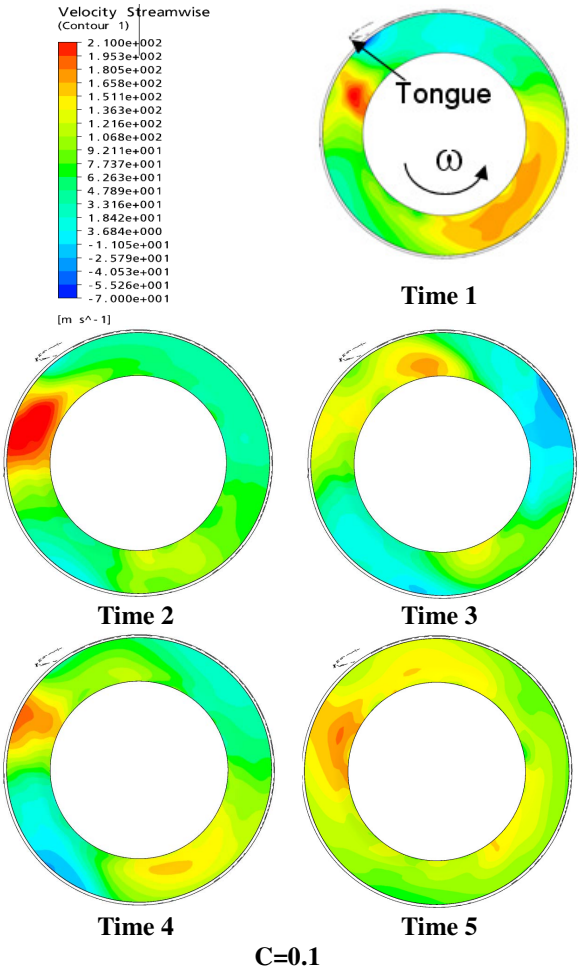

Fig. 10 Radial velocity contours in diffuser at five time instants

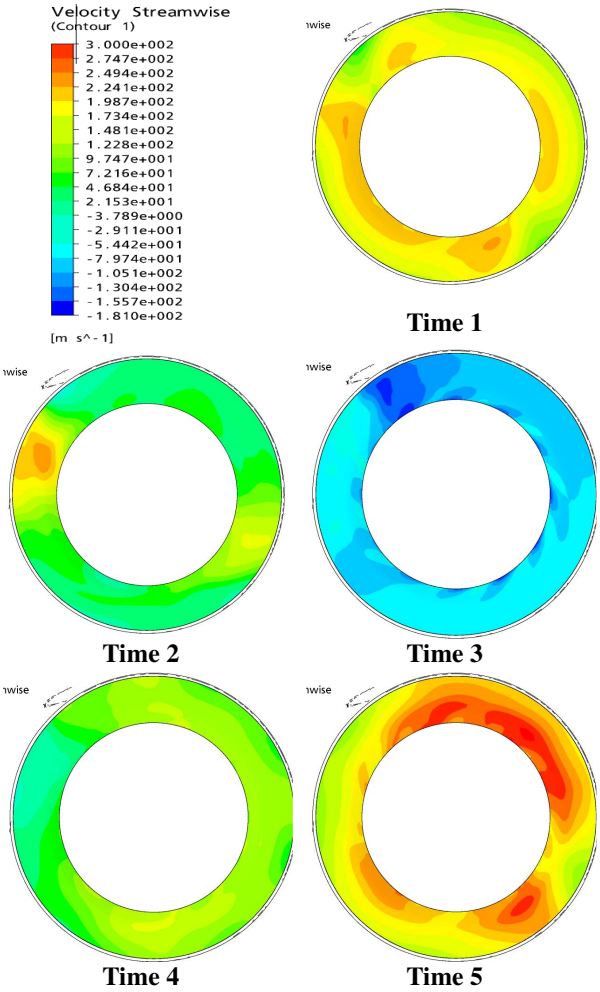

C=0.05712

Fig. 10 Cont'd

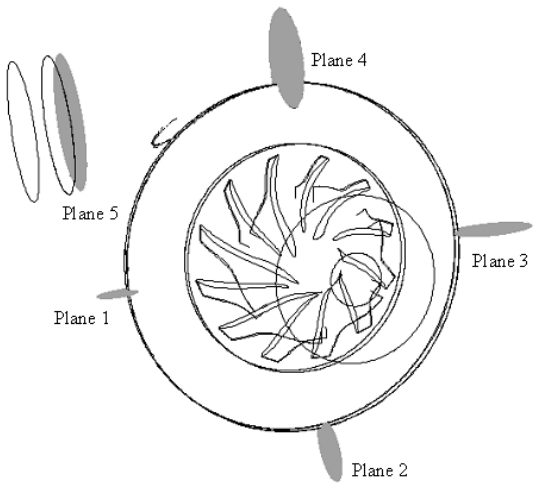

Fig. 11 Five volute cross sections

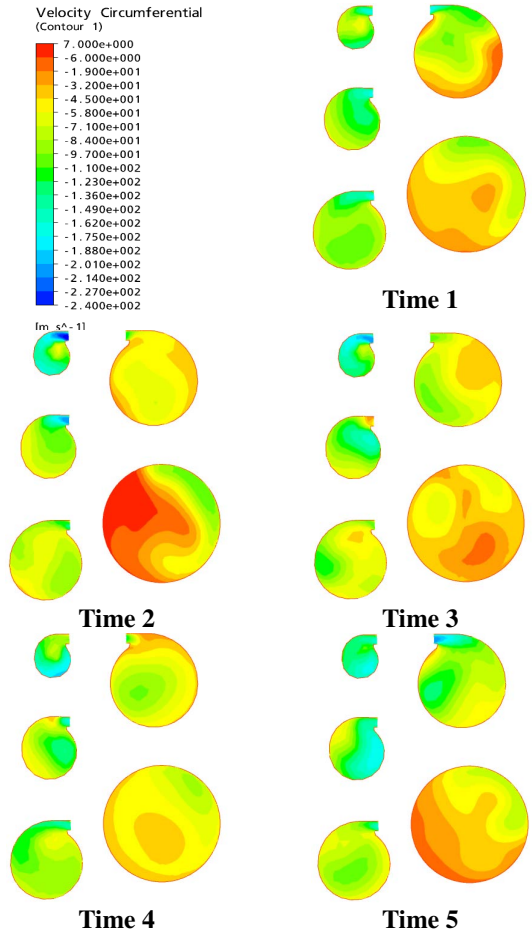

C=0.1

Fig. 12 Circumferential velocity contours in volute at five time instants

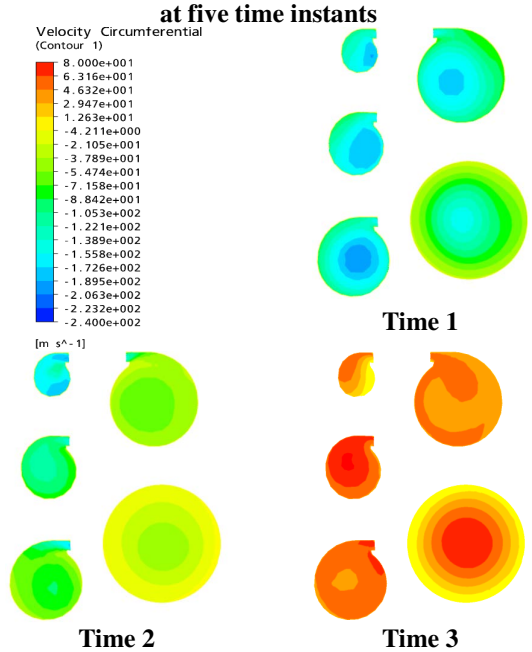

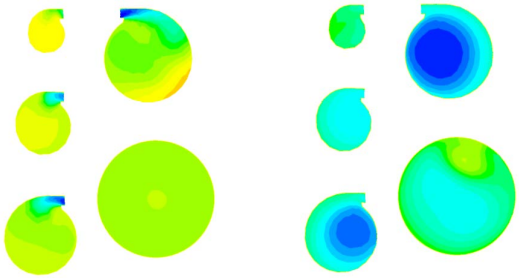

Time 4 **Time 5**

C=0.05712

Fig. 12 Cont'd

The swirl velocity vectors at the five tangential locations in the volute at the five time instants are given in **Fig. 13**. When the C value is 0.1 and at most time instants, from cross sections 1 to 4, a single vortex is observed, which is typical for a volute with a tangential inlet. The movement of the vortex center at the cross sections along the tangential direction coincides with the movement of the low static pressure center[23], and is therefore associated with the through flow and circumferential curvature of the volute. But in the cross section 5, the driving force behind the vortex flow vanishes so the swirl velocity decreases due to flow mixing. This is accompanied by a vortex breaking down at the cross section center. The breaking down of the vortex center is caused by the instability of the swirling flow[26, 27] in the volute and when it happens the vortex center breaks up into smaller vortex pairs. Break down of the vortex also occurs at cross section 4 at time instants 4 and 5 when the mass flow at the compressor inlet is increasing. But when the C value is 0.05712, vortex distortion and break down cannot be seen at time instants 1 and 2, while at time instants 3 and 4, the swirl velocity almost dies out.

5. Discussions

3D Navier-Stokes equations and the k-ε turbulence model was applied to a turbocharger compressor with two different sizes (0.0909 m^3 and 0.1591m^3) of downstream plenums at a measured surge mass flow rate. The results show that with the larger plenum the compressor went into surge at a dominating frequency of 22.6Hz, while the surge cycle was far less clear with the smaller plenum, and dominating frequency increased to 71.6Hz.

With the larger plenum, the impeller passage flow was axisymmetric and responsed to the 22.6Hz unsteadiness in a quasi-steady manner. With the smaller plenum however, the flow was less axisymmetric and displayed some features of a rotating stall.

With the smaller plenum, the diffuser flow showed standing-wave features but there were no such features with the larger plenum.

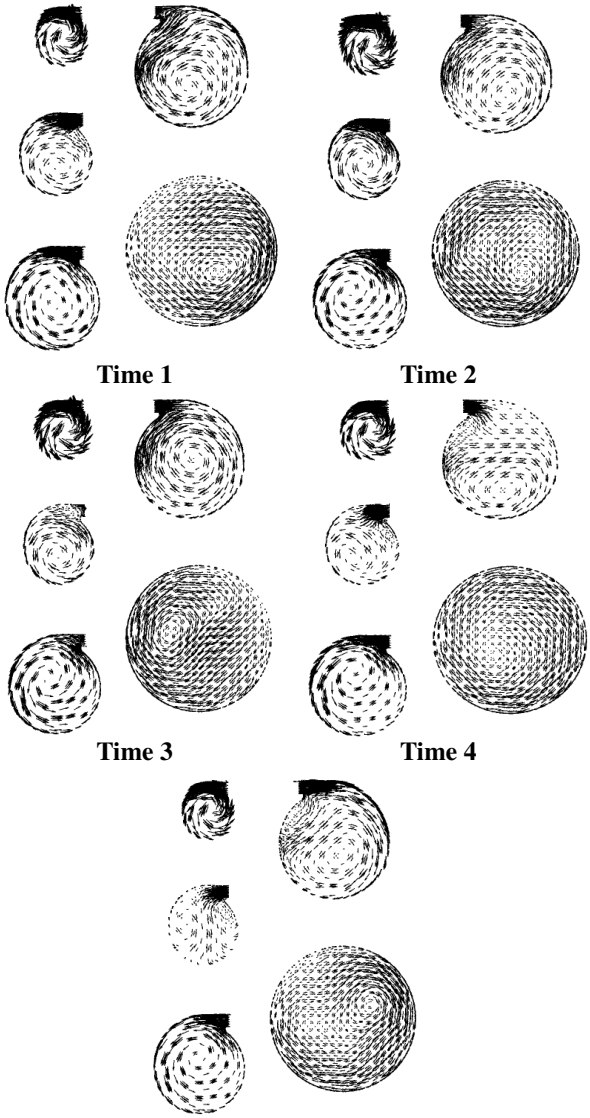

Time 1 **Time 2**

Time 3 **Time 4**

Time 5

C=0.1

Fig. 13 Swirl velocity vectors in volute at five time instants

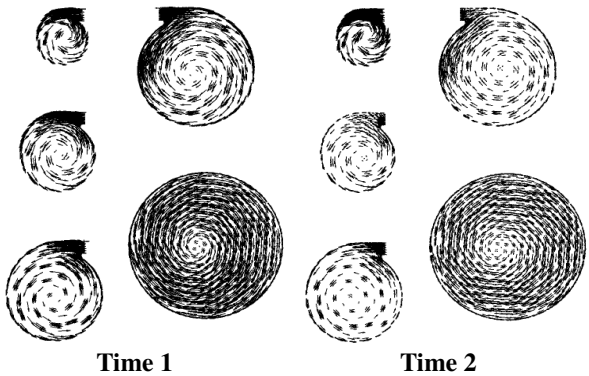

Time 1 **Time 2**

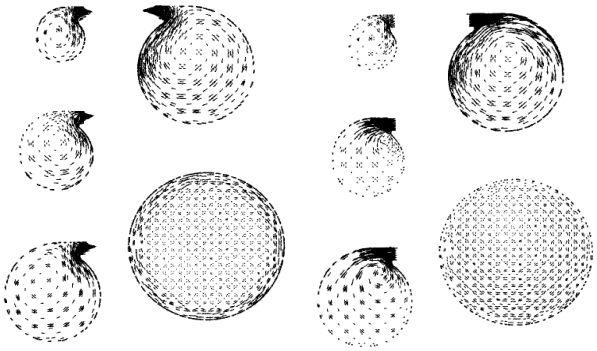

Time 3 **Time 4**

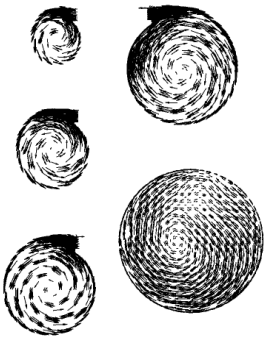

Time 5
C=0.05712
Fig. 13 Cont'd

The through flow in the volute showed strong reversing flow with the larger plenum, the flow was also more regular at the volute cross sections. Total vortex break down in the sections were synchronised with inlet mass flow oscillation. With the smaller plenum, the reversing flow in the volute was less severe, less uniform or less regular, and the vortex break down only occurred at the centers of the larger cross sections. Both through flow and vortex flow showed phase differences from the inlet mass flow oscillation.

This work demonstrates the value of CFD in study of instabilities of centrifugal compression systems. It would be useful to extend the work to include the influence of inlet piping. Such work is currently under taken. It would also be extremely valuable if a better stall and surge model could be developed for centrifugal compression systems as applications of the Moore-Greitzer model for such systems are still unsatisfactory.

6. Acknowledgments
The authors are grateful to Honeywell Inc. for permission to publish this paper.

References

1. Moore F.K., Greitzer E.M. (1986), A Theory of Post-Stall Transients in Axial Compression Systems: Part 1-Development of Equations, Journal of Engineering for Gas Turbines and Power, 108, 68-76.
2. Greitzer E.M., Moore F.K. (1986), A Theory of Post-Stall Transients in Axial Compression Systems: Part II—Application, Journal of Engineering for Gas Turbines and Power, 108, 231-239.
3. Mezic I., A large-scale theory of axial compression system dynamics, Journal of Fluid Dynamics, 2000.
4. Birnir B. Hou S.M. and Wellander N., Derivation of the viscous Moore-Greitzer equations for aeroengine flow, Center for Complex and Nonlinear Science, University of California Santa Barbara, eScholarship, 1st January 2007.
5. Fink, D. A., Cumpsty, N. A., and Greitzer, E. M. (1992). Surge Dynamics in a Free-Spool Centrifugal-Compressor System, Journal of Turbomachinery-Transactions of the ASME, 114(2), 321-332.
6. Gravdahl, J. T., and Egeland, O. (1999). Compressor surge and rotating stall: Modelling and control, Springer, London; New York.
7. Kang, J.-S., and Kang, S.-H. (2003). Stall inception in a vaneless diffuser of a centrifugal compressor. ASME Turbo Expo 2003, GT-2003-38358.
8. Levy, Y., and Pismenny, J. (2003). The number and speed of stall cells during rotating stall." ASME Turbo Expo 2003, GT-2003-38221.
9. Longley, J. P. (1994). A Review of Nonsteady Flow Models for Compressor Stability. Journal of Turbomachinery-Transactions of the ASME, 116(2), 202-215.
10. Paduano, J. D., Greitzer, E. M., and Epstein, A. H. (2001). Compression system stability and active control. Annual Review of Fluid Mechanics, 33, 491-517.
11. Senoo, Y., Kinoshita, Y., and Ishida, M. (1977). Asymmetric Flow in Vaneless Diffusers of Centrifugal Blowers. Journal of Fluids Engineering-Transactions of the ASME, 99(1), 104-114.
12. Spakovszky, Z. S. (2004). Backward traveling rotating stall waves in centrifugal compressors. Journal of Turbomachinery-Transactions of the ASME, 126(1), 1-12.
13. Greitzer, E. M. (1981). The Stability of Pumping Systems - the 1980 Freeman Scholar Lecture." Journal of Fluids Engineering-Transactions of the ASME, 103(2), 193-242.
14. Rose, M., Irmler, K., Schleer, M., and Abhari, R. S. (2003). Classic surge in a centrifugal compressor. ASME Turbo Expo 2003, GT 2003-38476.
15. Matthias Schleer, Reza S. Abhari. (2005). Influence of geometric scaling on the stability and range of a turbocharger centrifugal compressor. ASME Turbo Expo 2005, GT2005-68713
16. Wernet P. M., Bright M. M. and Skoch J. G., An investigation of surge in a high-speed centrifugal compressor using digital PIV, Journal of Turbomachinery, Trans. ASME, Vol 123, 418-428, April 2001.

17. Rivera, C. J., Numerical Simulation of Dynamic Stall Phenomena in Axial Flow Compressor Blade Rows," Ph.D. Dissertation, Georgia Institute of Technology, 1998.
18. Escuret, J. F., Garnier, V., Numerical Simulations of Surge and Rotating-Stall in Multi-Stage Axial-Flow Compressors, AIAA Paper 94-3202, 1994.
19. He, L., Computational Study of Rotating Stall Inception in Axial Compressor, Journal of Propulsion and Power, Vol. 13, No. 1, pp. 31-38, Jan.-Feb. 1997.
20. Niazi S, Stein A & Sankar L N. Numerical Studies of Stall and Surge Alleviation in a High-Speed Transonic Fan Rotor, AIAA Paper 2000-0225, 2000.
21. Saeid Niazi. Numerical Simulation of Rotating Stall and Surge Alleviation in Axial Compressors. Doctor Thesis, Georgia Institute of Technology, USA, 2000.
22. M. Vahdati, G. Simpson and M. Imregun, Unsteady Flow And Aeroelasticity behaviour of Aero-Engine Core Compressors During Rotating Stall And Surge, ASME Turbo Expo 2006, GT2006-90308
23. Guo Q, Chen H et al, Numerical simulations of stall inside a centrifugal compressor, Proceedings of the Institution of Mechanical Engineers, Part A, Journal of Power and Energy, Vol. 221(5), pp. 683-693, 2007.
24. Chen H, Guo Q et al, Numerical Simulations of Onset Of Volute Stall Inside a Centrifugal Compressor, ASME Turbo Expo 20086, GT2008-50036
25. CFX user guide, version 12.0. CFX Ltd, 2009.
26. Yin X Y, Sun D J, Vortex stability. (In Chinese), 2003, ISBN 7-118-02897-5.
27. Greitzer E M, Tan C S and Graf M B, Internal Flow, Cambridge University Press, 2004, ISBN 0-521-34393-3.